MESH-BASED SPHERICAL DECONVOLUTION FOR PHYSICALLY VALID FIBER ORIENTATION RECONSTRUCTION VIA DIFFUSION-WEIGHTED MRI

Vishal Patel, Yonggang Shi, Paul Thompson, Arthur Toga

Laboratory of NeuroImaging
University of California, Los Angeles

ABSTRACT

High angular resolution diffusion imaging (HARDI) methods have enabled the reconstruction of complex spin diffusion profiles in central nervous system white matter through diffusion-weighted MRI. For recovery of the underlying fiber orientations, conventional spherical deconvolution techniques based on spherical harmonics typically have difficulty producing fiber orientation distributions (FODs) that simultaneously satisfy the physical constraints of being real, symmetric, and non-negative. In this work, we propose a novel approach for HARDI reconstruction that is guaranteed to generate FODs satisfying these constraints. By using a meshed representation of the unit sphere, we formulate the spherical deconvolution as a convex optimization problem and compute the solution using a projected gradient descent algorithm. Flexible regularization is also included in our method to allow for tuning the sharpness of the reconstructed FOD. In our experiments, we present simulated results to examine the effects of varying the regularization parameters, and we illustrate the robustness of our method by applying it to several biological data sets to reconstruct known white matter fiber geometry.

***Index Terms*—** Deconvolution, magnetic resonance imaging, inverse problems, optimization methods, brain

1. INTRODUCTION

Diffusion-weighted magnetic resonance imaging (DW-MRI or DWI) has enabled the measurement of spin diffusion characteristics on a voxel-by-voxel basis. A variety of methods exist for estimating the spin diffusion propagator, from the simple but widely-used diffusion tensor imaging (DTI) methods, which implicitly assume only a single fiber population in each voxel, to more complex, model-independent HARDI methods such as diffusion spectrum imaging (DSI), q-ball imaging (QBI), and persistent-angular-structure (PAS-MRI) [1, 2, 3, 4, 5].

For fiber tractography, however, the object most directly of interest is not the diffusion profile itself, but rather the underlying fiber geometry constraining the spin diffusion [6]. To recover this fiber orientation distribution, it is appropriate to interpret the measured DWI signal attentuation profile as a convolution of the complex underlying fiber geometry with some single-fiber response function (*i.e.*, the impulse response). Deconvolution using the appropriate kernel should then provide the desired FOD. Given its interpretation as a distribution of fiber orientations, the FOD should be a real, symmetric (assuming fiber radii of curvature are large relative to voxel dimensions), and non-negative function on S^2 [7].

The spherical deconvolution concept is closely related to the multi-tensor fitting approach used in several previous reports, but it has been shown that direct, model-independent spherical deconvolution outperforms these methods, particularly in voxels containing multiple fiber populations [6, 8, 9]. Nevertheless, deconvolution is an ill-posed inverse problem, and previously reported algorithms have demonstrated difficulty generating solutions which simultaneously satisfy the realness, symmetry and non-negativity constraints. In particular, the non-negativity criterion has proven difficult to guarantee for approaches utilizing a spherical harmonics-based representation of the signal attenuation and FOD [7]. Even Tournier *et al.*'s recent procedure for constrained spherical deconvolution (CSD) merely penalizes negative values in the solution rather than explicity forbidding them [6].

In this report, we reformulate the deconvolution on a dense, discrete spherical mesh. We show how this formulation enables solution of the deconvolution problem in a principled and predictable manner while also guaranteeing FOD solutions which are physically valid. Moreover, we include flexible regularization terms in our formulation, and we examine the effects of varying these parameters. Finally, we apply our methods to real DWI data sets and demonstrate robust recovery of known fiber anatomy.

2. METHODS

2.1. Mesh-based spherical deconvolution

The spherical harmonics (assuming an infinite number of coefficients) form a complete basis for complex-valued functions on the sphere S^2. We recognize, however, that although

This work was supported by the National Institutes of Health through grants 1U54RR021813-01 (Center for Computational Biology) and 5T32GM008042-25 (Medical Scientist Training Program).

use of these functions may simplify the representation of the FOD and signal attentuation profile by mapping them into the frequency domain, imposing space domain constraints such as non-negativity within this framework becomes exceedingly complicated. Thus, we choose instead to formulate the deconvolution problem on a dense hemispherical mesh. Assuming m measured DWI signal attenuations, and an n-point mesh:

$$\hat{\mathbf{x}} = \underset{\mathbf{x}}{\operatorname{argmin}} \left(\|\mathbf{A}\mathbf{x} - \mathbf{b}\|_2^2 + \tau \|\mathbf{D}\mathbf{x}\|_p^p \right);\ \mathbf{x} \geq \mathbf{0}, p \geq 1 \quad (1)$$

where $\mathbf{x}$ is the n-dimensional FOD estimate, $\mathbf{A}$ is an $m \times n$ convolution matrix, $\mathbf{b}$ is an m-dimensional vector containing the signal attenuations, and τ, $\mathbf{D}$, and p are regularization parameters described further below.

Equation 1 casts the deconvolution as a convex optimization problem. The data-driven term $\|\mathbf{A}\mathbf{x} - \mathbf{b}\|_2^2$ seeks the least-squares-optimal solution by imposing a penalty according to the difference between the measured signal attenuations $\mathbf{b}$ and the FOD estimate projected through $\mathbf{A}$ onto the m diffusion weighted gradient directions. $\mathbf{A}$ is formed columnwise by rotating the single-fiber response function to align with each of the n mesh directions, and then sampling the rotated function on the m measurement directions. The single-fiber response function itself is determined, as in previous reports, directly from the data by aligning and averaging the signal attenutation profiles from the 300 voxels in the volume with the highest generalized fractional anisotropy (GFA) [4, 6, 7].

The regularization term in Equation 1, $\tau \|\mathbf{D}\mathbf{x}\|_p^p$, allows the FOD estimate to be biased in terms of the properties encompassed in the regularization matrix $\mathbf{D}$. Typically, one desires a smooth FOD solution, so $\mathbf{D}$ can be chosen—as for all experiments in this report—to be a simple difference matrix over neighboring vertices on the spherical mesh. Alternatively, if one favors a sparse solution, $\mathbf{D}$ may be set equal to the identity. The parameter τ controls the relative weighting of the regularization term and the data-driven term, while p provides p-norm control over the strength of the regularization penalty term $\mathbf{D}\mathbf{x}$.

2.2. Projected gradient descent

Since Equation 1 characterizes a convex optimization problem, we can obtain a solution via gradient descent. We begin with an initial guess $\mathbf{x_0} = \mathbf{A^+ b}$, where $\mathbf{A^+}$ signifies a pseudoinverse obtained via truncated singular value decomposition. We then proceed with the iterative process of stepping in the direction of the negative gradient. If the argument in Equation 1 is denoted as $f(\mathbf{x})$, the gradient is:

$$\nabla f(\mathbf{x}) = \mathbf{A^T A x} + \tau p \mathbf{D^T} \left(\mathbf{D x} \cdot |\mathbf{D x}|^{p-2} \right) \quad (2)$$

where the exponentiation and the multiplication indicated by $(\cdot)$ are carried out element-wise. We perform a line search along this direction to determine the optimal step length δ and then update the FOD estimate according to:

$$\mathbf{x_{t+1}} = \max\left(\mathbf{x_t} - \delta \nabla f(\mathbf{x_t}), \mathbf{0}\right) \quad (3)$$

where we have projected the FOD estimate onto the non-negative space to ensure that the final solution $\hat{\mathbf{x}}$ satisfies its physical constraints. We choose to cease iterating when the J-divergence (symmetrized KL-divergence) between successive FOD estimates falls below a certain threshold, set for this report to be 1×10^{-8} for a 1281-directional hemispherical mesh. The value of the FOD on each hemispherical vertex is then reflected across the origin to complete the sphere and simultaneously satisfy the symmetry constraint.

2.3. Simulated data

To better understand the properties of our mesh-based formulation, we analyzed its behavior when applied to simulated voxels. These data sets were generated using the previously-reported multi-tensor model, derived from the Stejskal-Tanner equations:

$$\mathbf{s}(\mathbf{u_j}) = s_0 \sum_q f_q e^{-b \mathbf{u_j^T D_q u_j}} + \eta \quad (4)$$

where the DWI signal for gradient direction $\mathbf{u_j}$ is a weighted sum of contributions from each fiber [10]. All simulated fibers were assumed to generate a prolate diffusion profile, such that the eigenvalues of the diffusion tensor $\mathbf{D_q}$ were fixed as $\lambda_1 = 1.7 \times 10^{-3}\text{mm}^2/\text{s}$ and $\lambda_2 = \lambda_3 = 0.2 \times 10^{-3}\text{mm}^2/\text{s}$. For this report, the b-value was chosen to be $1000\text{s}/\text{mm}^2$, and the complex Gaussian noise η was chosen from a distribution with width $\sigma = 1/\text{SNR}$.

2.4. Real data acquisition

Real data sets were acquired at the Center for Magnetic Resonance at the University of Queensland using a 4 Tesla Bruker Medspec scanner with a transverse electromagnetic (TEM) headcoil. Diffusion-weighted scans utilized a single-shot echo planar technique with a twice-refocused spin echo sequence to minimize eddy-current induced distortions. The timing of the diffusion sequence was optimized for SNR. 94 diffusion-sensitized gradient directions and 11 baseline images with no diffusion-sensitization were obtained for every subject. Imaging parameters were: b-value = 1159 s/mm^2, TE/TR = 92.3/8,259 ms, FOV = 230 $\times$ 230, voxel size = 1.8 mm $\times$ 1.8 mm $\times$ 2.0 mm, acquisition time = 14:30 min.

3. RESULTS

We first applied our mesh-based deconvolution algorithm to a data sets simulating two equally-weighted fibers crossing at 90°. These 60-directional synthetic data sets were generated using a realistic signal-to-noise ratio of SNR = 10. The convergence profile for a representative run for one of these simulations is shown in Figure 1, and confirms that Equation

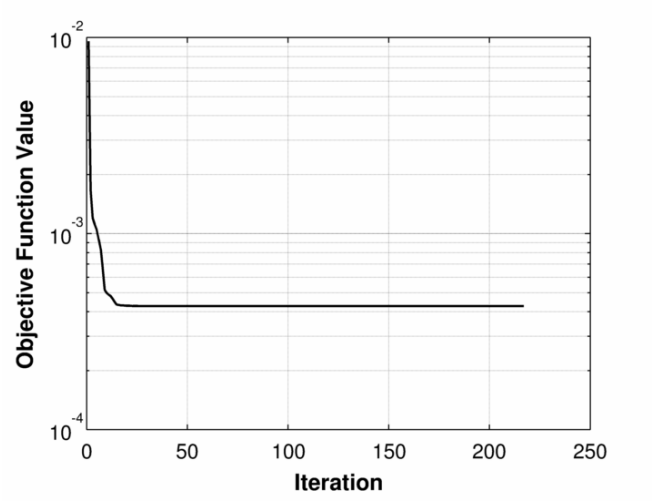

Fig. 1. Convexity of the mesh-based spherical deconvolution. A representative plot of the value of $\|\mathbf{Ax}-\mathbf{b}\|_2^2+\tau\|\mathbf{Dx}\|_p^p$ with respect to iteration for solution of a simulated 90° fiber crossing.

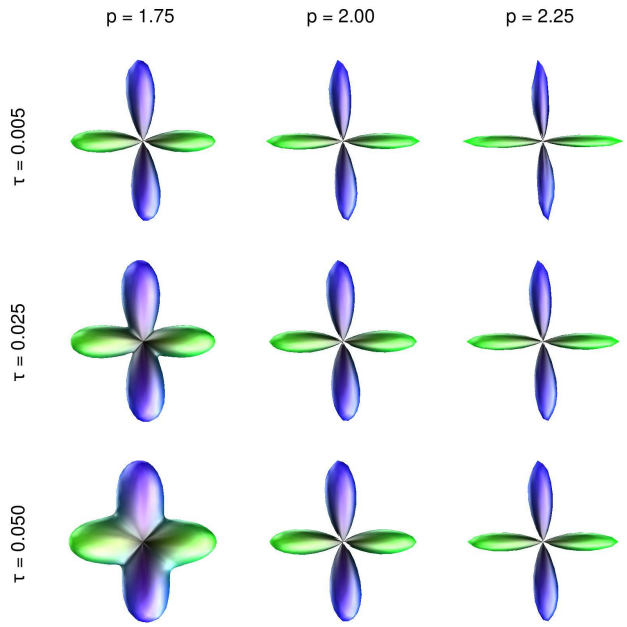

Fig. 2. Effect of regularization parameters on the deconvolution solution for a 60-directional simulated 90° fiber crossing with SNR $= 10$. Deconvolution results are shown for a range of $\tau = \{0.005, 0.025, 0.050\}$ (top to bottom) and $p = \{1.75, 2.00, 2.25\}$ (left to right).

1 is indeed convex. In addition, we note that the rate of convergence is initially rapid and decreases as the estimate approaches the global minimum, a behavior consistent with the known characteristics of gradient descent algorithms.

We also examined the effects of the regularization parameters τ and p on the shape of the FOD solution. Using the same 60-directional simulated data sets, we allowed τ to take on values $\{0.005, 0.025, 0.050\}$ and p to vary through $\{1.75, 2.00, 2.25\}$. As noted in Section 2.1, the regularization matrix $\mathbf{D}$ was defined as a difference matrix between neighboring vertices on the mesh. The results of solving Equation 1 using the projected gradient descent algorithm for each combination of regularization parameters are shown in Figure 2. We observe that increasing τ results in a smoother FOD solution, which is expected since we have chosen $\mathbf{D}$ to penalize large differences on neighboring mesh vertices. The sharpness of the FOD solution has a direct relationship with the magnitude of p as well. Although the commonly-recognized behavior of the p-norm is that lower values promote sparse or sharp solutions, we note that the reverse relationship is expected in this case since, by definition, all of the values in the penalty vector $\mathbf{Dx}$ are necessarily less than 1. Finally, we observe that the mesh-based deconvolution is not overly sensitive to the regularization parameters, since we are able to achieve acceptable FOD reconstructions for a range of p and τ, in the latter case over a full order of magnitude.

Having examined the characteristics of our mesh-based approach using simulations, we proceeded to verify its validity using real data sets. We applied the mesh-based spherical deconvolution algorithm to ten 94-directional DWI data sets acquired from healthy human subjects in an attempt to reconstruct known fiber anatomy. Guided by the results from Figure 2, we selected regularization parameters $\tau = 0.025$ and $p = 2.25$ for reasonably sharp fiber reconstructions, and left these values unchanged for all data sets. Using the mesh-based spherical deconvolution approach, we were able to obtain real, symmetric, and non-negative FOD reconstructions for every voxel in all ten data sets, as guaranteed by the formulation. To illustrate the recovery of known fiber anatomy, we present in Figure 3 characteristic reconstructions from three data sets of the intersection between the corpus callosum and corticospinal tracts in coronal section. This intersection is difficult to resolve with conventional DTI, but as we have shown, spherical deconvolution clearly illustrates the presence of voxels containing crossing fibers in this region. Moreover, the fact that we were able to resolve this intersection in all ten data sets without tuning of the regularization parameters illustrates the robustness and stability of our approach.

4. CONCLUSIONS

We have defined and demonstrated a novel mesh-based method for spherical deconvolution for the recovery of fiber orientations from DWI signal volumes. In contrast to previous methods, our procedure is guaranteed by formulation to produce real-valued, symmetric, and non-negative solutions in compliance with the physical constraints on the FODs. In addition, we have demonstrated how manipulation of the regularization parameters in our model allows for control

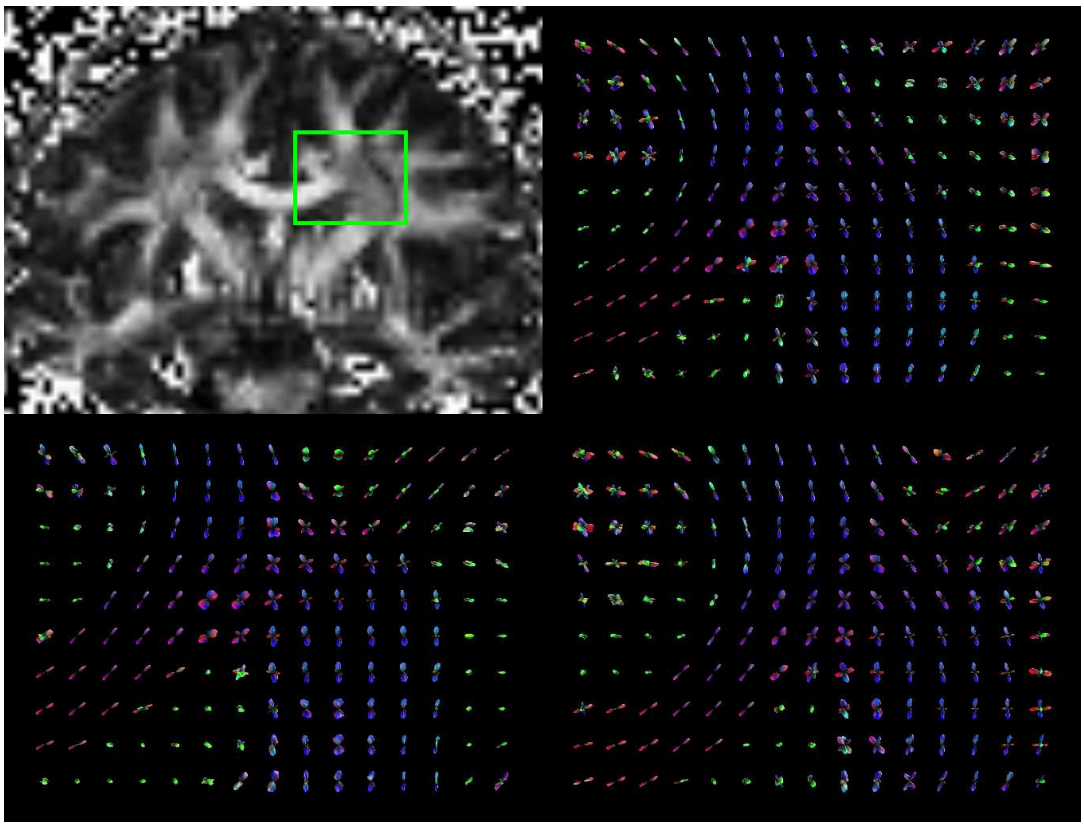

Fig. 3. Results of mesh-based spherical deconvolution on real data sets. The representative fractional anisotropy map at top-left highlights the region (boxed) corresponding to the intersection between the corpus callosum and corticospinal tracts for which FOD results are shown in the other three panels for different subjects. Voxels containing crossing fibers are clearly discernable at the intersections. All real data sets were evaluated with the same regularization parameters ($\tau = 0.025$, $p = 2.25$).

over the sharpness of the fiber orientation reconstruction. Finally, we have confirmed the validity and robustness of our approach by demonstrating its ability to accurately recover known fiber crossing geometry from several real data sets without the need for parameter tuning. The mesh-based spherical deconvolution method thus provides a principled and powerful technique for the determination of white matter fiber orientations which we expect will be useful for tractography and segmentation algorithms.

5. REFERENCES

[1] P. J. Basser, J. Mattiello, and D. LeBihan, "MR diffusion tensor spectroscopy and imaging," *Biophys. J.*, vol. 66, pp. 259–267, Jan 1994.

[2] L. R. Frank, "Characterization of anisotropy in high angular resolution diffusion-weighted MRI," *Magn Reson Med*, vol. 47, pp. 1083–1099, Jun 2002.

[3] K. M. Jansons and D. C. Alexander, "Persistent Angular Structure: new insights from diffusion MRI data. Dummy version," *Inf Process Med Imaging*, vol. 18, pp. 672–683, Jul 2003.

[4] D. S. Tuch, "Q-ball imaging," *Magn Reson Med*, vol. 52, pp. 1358–1372, Dec 2004.

[5] V. J. Wedeen, P. Hagmann, W. Y. Tseng, T. G. Reese, and R. M. Weisskoff, "Mapping complex tissue architecture with diffusion spectrum magnetic resonance imaging," *Magn Reson Med*, vol. 54, pp. 1377–1386, Dec 2005.

[6] J. D. Tournier, F. Calamante, and A. Connelly, "Robust determination of the fibre orientation distribution in diffusion MRI: non-negativity constrained super-resolved spherical deconvolution," *Neuroimage*, vol. 35, pp. 1459–1472, May 2007.

[7] J. D. Tournier, F. Calamante, D. G. Gadian, and A. Connelly, "Direct estimation of the fiber orientation density function from diffusion-weighted MRI data using spherical deconvolution," *Neuroimage*, vol. 23, pp. 1176–1185, Nov 2004.

[8] D. S. Tuch, T. G. Reese, M. R. Wiegell, N. Makris, J. W. Belliveau, and V. J. Wedeen, "High angular resolution diffusion imaging reveals intravoxel white matter fiber heterogeneity," *Magn Reson Med*, vol. 48, pp. 577–582, Oct 2002.

[9] T. E. Behrens, H. J. Berg, S. Jbabdi, M. F. Rushworth, and M. W. Woolrich, "Probabilistic diffusion tractography with multiple fibre orientations: What can we gain?," *Neuroimage*, vol. 34, pp. 144–155, Jan 2007.

[10] D. C. Alexander, G. J. Barker, and S. R. Arridge, "Detection and modeling of non-Gaussian apparent diffusion coefficient profiles in human brain data," *Magn Reson Med*, vol. 48, pp. 331–340, Aug 2002.